Cell Reports
Methods

Article

Single-cell deep phenotyping of cytokine release unmasks stimulation-specific biological signatures and distinct secretion dynamics

Graphical abstract

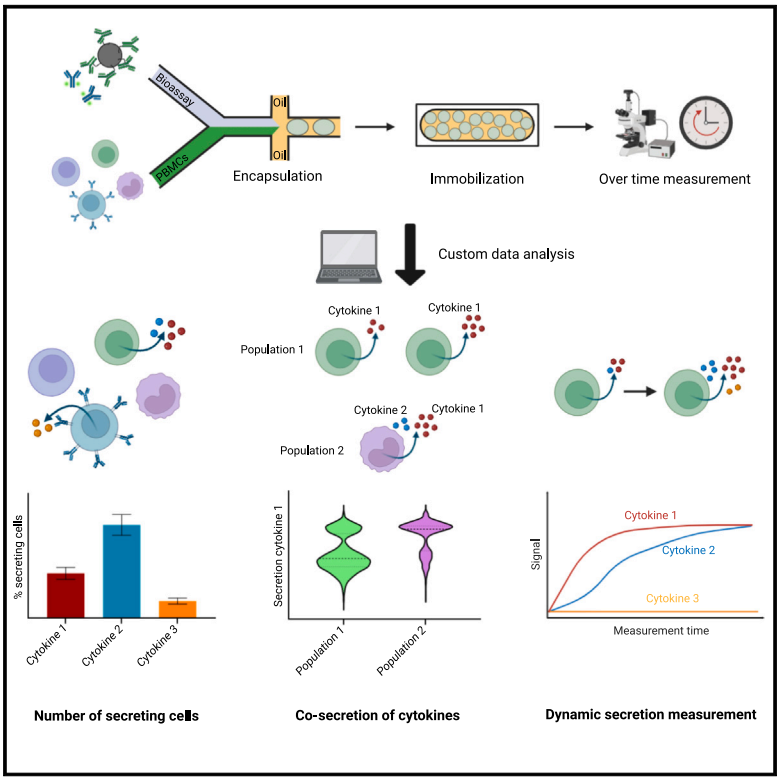

Highlights

- Microfluidic analysis of parallel cytokine release at the single-cell level over time
- Enhanced resolution revealed distinct early and late cytokine (co)secretion dynamics
- Visualization of stimulation-specific secretion signatures from human PBMCs

Authors

Kevin Portmann, Aline Linder, Nicole Oelgarth, Klaus Eyer

Correspondence

klaus.eyer@pharma.ethz.ch

In brief

Portmann et al. describe a method for the microfluidic measurement of dynamic cytokine co-secretion from single cells. The method is applied to study early and late stimulation responses in human PBMCs and reveals distinct stimulation-specific signatures and dynamics.

Portmann et al., 2023, Cell Reports Methods 3, 100502
July 24, 2023
https://doi.org/10.1016/j.crmeth.2023.100502

CellPress

Cell Reports Methods

CellPress
OPEN ACCESS

Article

Single-cell deep phenotyping of cytokine release unmasks stimulation-specific biological signatures and distinct secretion dynamics

Kevin Portmann,[1] Aline Linder,[1] Nicole Oelgarth,[1,2] and Klaus Eyer[1,3,*]

[1]Laboratory for Functional Immune Repertoire Analysis, Institute of Pharmaceutical Sciences, Department of Chemistry and Applied Biosciences, ETH Zürich, 8093 Zürich, Switzerland

[2]Present address: Laboratory for Cancer Immunology, Department of Biomedicine, University of Basel and University Hospital Basel, 4031 Basel, Switzerland

[3]Lead contact

*Correspondence: klaus.eyer@pharma.ethz.ch

https://doi.org/10.1016/j.crmeth.2023.100502

MOTIVATION Current cytokine release assays require a long incubation time and do not provide dynamic resolution over time on the single-cell level, masking potential alterations in the release and its dynamic evolution. Our single-cell microfluidic method combines a quantitative and fast readout with dynamic resolution in cytokine release. These added parameters could help in preclinical and clinical development to gain novel insights into the pathology of cytokine-inducing/induced diseases, stratify patients, and gain more insights into mechanisms of action of novel immune-therapeutic concepts.

SUMMARY

Cytokines are important mediators of the immune system, and their secretion level needs to be carefully regulated, as an unbalanced activity may lead to cytokine release syndromes. Dysregulation can be induced by various factors, including immunotherapies. Therefore, the need for risk assessment during drug development has led to the introduction of cytokine release assays (CRAs). However, the current CRAs offer little insight into the heterogeneous cellular dynamics. To overcome this limitation, we developed an advanced single-cell microfluidic-based cytokine secretion platform to quantify cytokine secretion on the single-cell level dynamically. Our approach identified different dynamics, quantities, and phenotypically distinct subpopulations for each measured cytokine upon stimulation. Most interestingly, early measurements after only 1 h of stimulation revealed distinct stimulation-dependent secretion dynamics and cytokine signatures. With increased sensitivity and dynamic resolution, our platform provided insights into the secretion behavior of individual immune cells, adding crucial additional information about biological stimulation pathways to traditional CRAs.

INTRODUCTION

Cytokines are important mediators of the innate and adaptive immune system, responsible for mounting and controlling an appropriate immune response.[1] The immune system must trigger cytokine secretion in response to infections to appropriately deal with and ultimately eliminate the threat.[2,3] However, the activation and cytokine secretion levels must be well balanced, as unnecessary and overshooting responses are associated with metabolic costs and tissue damage due to systemic inflammation, known as cytokine release syndrome (CRS).[4,5] Irregular cytokine secretion patterns and CRS have been associated with many diseases and conditions, including COVID-19, HIV, and childhood obesity.[6–9] Therefore, the cytokine secretion level and dynamic control thereof are vital for homeostasis in health and disease.

Unwanted and unbalanced cytokine release can also be triggered by molecules used for therapeutic purposes, such as proteins interacting with crucial receptors in the immune system and cellular therapies.[10–14] Therefore, *ex vivo* cytokine stimulation assays play a crucial role in drug development as part of predictive immunotoxicology (ITOX) to assess the potential cytokine-inducing side effects of drugs in early preclinical development.[15,16] Indeed, regulatory pressure increased to mandate these assays in the aftermath of the TGN1412 phase 1 study in 2006, where the tested anti-CD28 superagonist antibody led to the induction of severe cytokine release and multi-organ failure.[17,18] In these so-called cytokine release assays (CRAs), human peripheral blood

mononuclear cells (PBMCs) or whole blood is stimulated *ex vivo* by the therapeutic molecule and appropriate controls.[19–23] The most frequently used assays mainly differ in the stimulation used, involving either the drug coated as a solid substrate or added in solution.[20] Results are usually reported at a given time as a concentration in the supernatant or as a percentage of activated, cytokine-secreting cells (CSCs) determined by ELISpot.[24] However, many of the recently developed, immune-based therapies in cancer and immune-related diseases must induce a certain level of cytokine release to be beneficial. Therefore, the level of cytokine release and its dynamic control are important factors in assessing whether a therapy stimulates or overstimulates the immune system. While today's CRAs give quantitative information about cytokine secretion in bulk or the frequency of secreting cells, only a low-resolution understanding is often achieved considering cellular heterogeneity and the correlation, control, and differences in cellular secretion. Although cellular heterogeneity in cytokine release has been recently examined with ELISpot,[25] no dynamic observations or secretion level was extracted. Indeed, these potentially important parameters require a quantitative dynamic measurement on a single-cell level to be properly resolved.[26–28] Moreover, endpoint measurements might mask potential differences during secretion, which could give insights into the underlying biological activation and regulation in response to the stimulation.

To overcome the challenges described above, we established an advanced single-cell microfluidic-based cytokine secretion platform based on our initially developed platform DropMap.[29] In this system, individual cells were encapsulated into 65-pL water-in-oil droplets, where the small and controlled volume allowed for sensitive and quantitative detection of the secretion level for individual proteins of interest per single cell. Upon secretion, fluorescently labeled detection antibodies relocated onto the paramagnetic nanoparticles, where fluorescence relocation was later calibrated to secreted concentration and secretion rates. To study cytokine release in the current study, we first developed bioassays for seven cytokines and set up the measurement windows to match cellular secretion rates, which differed by over three logs within and in between cytokines. Second, we optimized panels to measure up to three cytokines in parallel, extracting frequencies of secreting and co-secreting cells, individual secretion rates, and amounts, all with dynamic information, relying on a newly established data-analysis pipeline to analyze cellular cytokine secretion dynamics and co-secretion in parallel. We applied the assay to study well-described stimulants in a solution-based CRA in bulk using PBMCs, allowing the detection of differently responding cellular subpopulations and different dynamics based on the used stimulant (Figure 1A). This allowed us to quantitatively assess cytokine secretion and to monitor and study the dynamics behind cytokine secretion in response to various stimuli, unmasking the dynamic nature behind cytokine release on the single-cell level.

RESULTS

Establishment of cellular secretion measurements, parallelization, and dynamic readout

Previous applications of the DropMap platform focused on measuring a single protein species from purified cell populations, such as antibodies from splenic and bone marrow B cells or tumor necrosis factor α (TNF-α) from enriched human monocytes.[29,30] To assess cytokine release comparable with classical CRAs, we adapted the platform to measure up to three cytokines in parallel for every individual cell in a heterogeneous mixture of PBMCs. First, sandwich immunoassays were established for TNF-α, interferon-γ (IFN-γ), interleukin-2 (IL-2), IL-6, IL-8, and macrophage inflammatory protein 1α (MIP-1α), allowing the detection of said cytokines through measurement of fluorescence relocation on the single-cell level (Figure 1). Next, these immunoassays were compiled into different panels, including functionalized nanoparticles against three different cytokines and the respective fluorescently labeled detection antibodies (see STAR Methods for more information). We adapted the assays to allow for a high dynamic range, since the secretion level of various cytokines differs in the heterogeneous mixture of PBMCs. This was done by adjusting the number of nanoparticles encapsulated per cytokine as well as changing the concentration of secondary fluorescently labeled antibodies to achieve sensitive detection (for more information, refer to Bounab et al.[29] and Table S1). For quantification, calibration curves were established with recombinant proteins to calibrate the measured relocations to concentrations (Figure S1) and calculate limits of detection (LODs) and the overall dynamic range. The established assays reached LODs in the lower nanomolar or higher picomolar range with maximal measurable concentrations of up to 80 nM (see Tables S2 and S3 for details on dynamic ranges and antibodies used).

Next, we assessed the levels of unspecific binding to calculate any crosstalk between the different cytokines (Figure S1B). Observed fluorescence crosstalks for both panels were below the calculated LODs for the respective cytokines, so no correction was performed. Working with rather high cell/droplet ratios (0.2–0.4), we assessed the influence of co-encapsulation in our assays by further analyzing the raw data: singlets, doublets, and multiplets of encapsulated cells were sorted and analyzed for lipopolysaccharide (LPS)-stimulated PBMCs (Figure S2A). For the assessed cytokines, manually sorted droplets showed no significant influence of multiple cell encapsulation on measured secretion rates (Figure S2B), indicating no bias resulting from co-encapsulation of multiple secreting cells due to the low frequency in the heterogeneous population in general. Therefore, we opted not to exclude doublets and multiplets from additional analysis.

Enhanced time and single-cell resolution revealed distinct early cytokine secretion dynamics upon LPS stimulation

To measure the short-term response of a heterogeneous cell population, we first stimulated PBMCs with LPS in bulk, determined the frequency of secreting cells after 4 h of measurement, and compared our results with more established methods such as ELISpot and supernatant measurements. Figure 2A displays the results from a typical response of human PBMCs after a 1-h stimulation with LPS for the cytokines TNF-α, IL-6, and IL-1β compared with unstimulated PBMCs. Indeed, the microfluidic experiment showed a significant increase in CSCs upon LPS stimulation (6.54% ± 0.85% vs. 0.79% ± 0.16%, p = 0.006 for

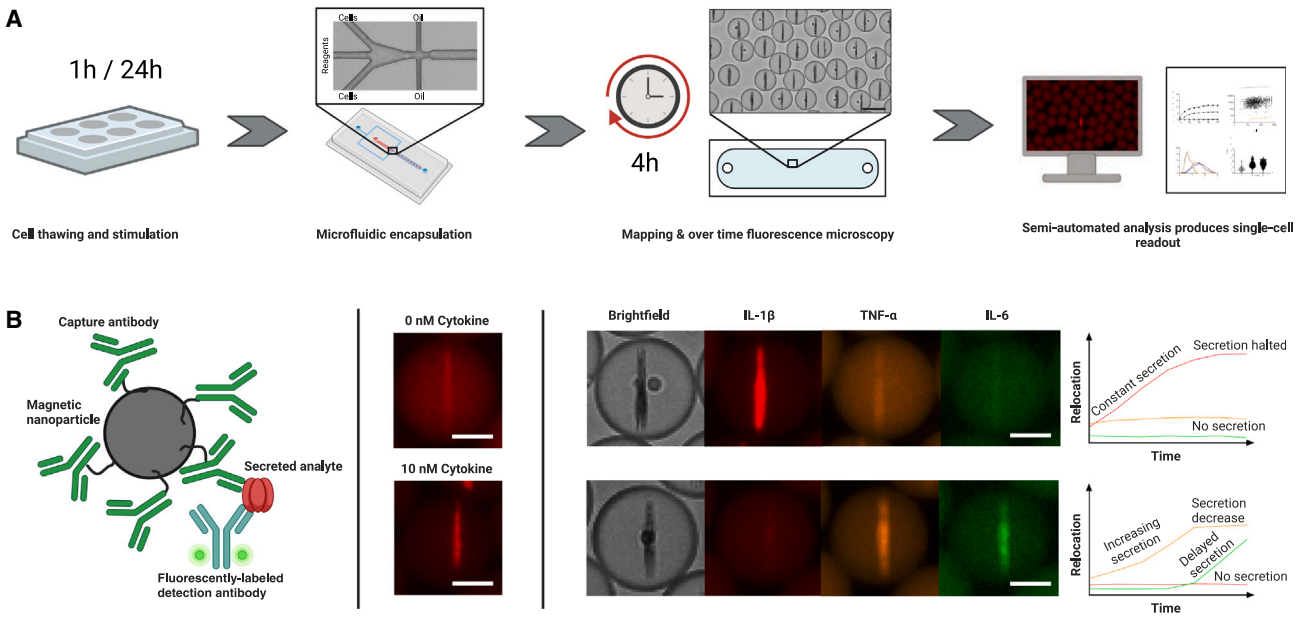

Figure 1. Experimental procedure and assay principle of the droplet-based single-cell multi-cytokine secretion measurement

(A) Overview of the experimental protocol. PBMCs were thawed and stimulated for the indicated time in bulk. Thereafter, the cells and assay reagents were randomly encapsulated in water-in-oil droplets with 65 pL volume (~50 μm diameter). Droplets were loaded into an observation chamber and continuously imaged with a fluorescence microscope over 4 h. The resulting images were analyzed as described in STAR Methods.

(B) Assay principle. PBMCs were co-encapsulated with assay reagents, i.e., (1) paramagnetic nanoparticles functionalized with anti-cytokine capture antibodies and (2) fluorescent-labeled anti-cytokine detection antibodies. Applying a magnetic field across the chamber aligned the particles to an elongated aggregate termed "beadline." The secretion of cytokines led to the capture of the secreted moiety on the particles and the subsequent relocation of the corresponding fluorescent detection antibody onto the beadline (second panel from left). Multiplexed cytokine measurements of individual cells were achieved by mixing nanoparticles functionalized against different cytokines with specific fluorochrome-labeled detection antibodies, as shown for representative cells secreting only IL-1β (top) and TNF-α + IL-6 (bottom). Owing to the static nature of the droplets over the 4-h measurement period, the fluorescence relocation can be measured for every individual cell (rightmost panel) over time. For more information, refer to STAR Methods. Scale bars, 25 μm.

Figure was created with BioRender.com.

TNF-α; 3.06% ± 0.52% vs. 0.21% ± 0.06%, p = 0.01 for IL-6; and 0.59% ± 0.16% vs. 0.02% ± 0.01%, p = 0.04 for IL-1β). One of the replicates was additionally measured using ELISpot. Although these methods are not directly comparable because of differences in incubation times, volumes, and the potential autocrine and paracrine responses (4-h in-droplet measurement vs. prolonged bulk incubation), a similar increase in the frequency of TNF-α-secreting cells was observed (4.6% for this replicate in droplets vs. 5.6% in ELISpot, Figure 2A). Interestingly, these results indicated that over 80% of the TNF-α-secreting cells detected after 24 h in the spot assay are already active after 1 h. This observation was in stark contrast to the unstimulated cells, with 0.4% in the droplets compared with 2.3% for the ELISpot, indicating that only roughly 20% of background activation occurred during the first hour. Supernatant measurements after 1 h of stimulation indicated the activation of TNF-α-secreting cells (Figure 2A, 84 ± 25 pg/mL vs. 6 ± 1 pg/mL [below LOD of the assay], p = 0.07). However, the supernatant measurement did not yield significant differences after 1 h compared with unstimulated cells owing to large variations in the concentration measured for stimulated cells.

We next evaluated assay variation and the influence of encapsulation on the cells by multiple measurements of the same cells (Figure S3). Here, we found that the impact of the stimulation on the percentage of activated cells for every cytokine was much stronger than the technical assay variation (and the influence the encapsulation had on the cells), as identified by comparison of coefficients of variation for the technical vs. biological replicates (0.02 vs. 0.34 for TNF-α, 0.07 vs. 0.47 for IL-6, and 0.06 vs. 0.78 for IL-1β, Figure S3). Therefore we concluded that the method was robust and suitable to measure differences, owing to the stimulation.

As the measurement time was fixed to 4 h, we next investigated whether this time was sufficient to detect all secreting cells (Figure 2B). Curve fits of the dynamics showed that for the detection of all IL-1β-secreting cells, a longer measurement time would be necessary (detection of half of all secreting cells after 40 min for TNF-α, 79 min for IL-6 and ~163 min for IL-1β). Therefore, while this method enabled us to detect virtually all TNF-α- and IL-6-secreting cells, the frequency of IL-1β would be underestimated with the current settings.

In addition to the frequency of CSCs, the microfluidic method allowed quantification of the average in-droplet concentration of the secreted cytokines and the average individual secretion rates (see STAR Methods). Clearly, different secretion dynamics can be observed for every cytokine in the measured PBMCs (Figure 2C). For TNF-α, we observed a linear increase in the secreting unstimulated cells (slope 0.16 ± 0.05 nM/min), whereas

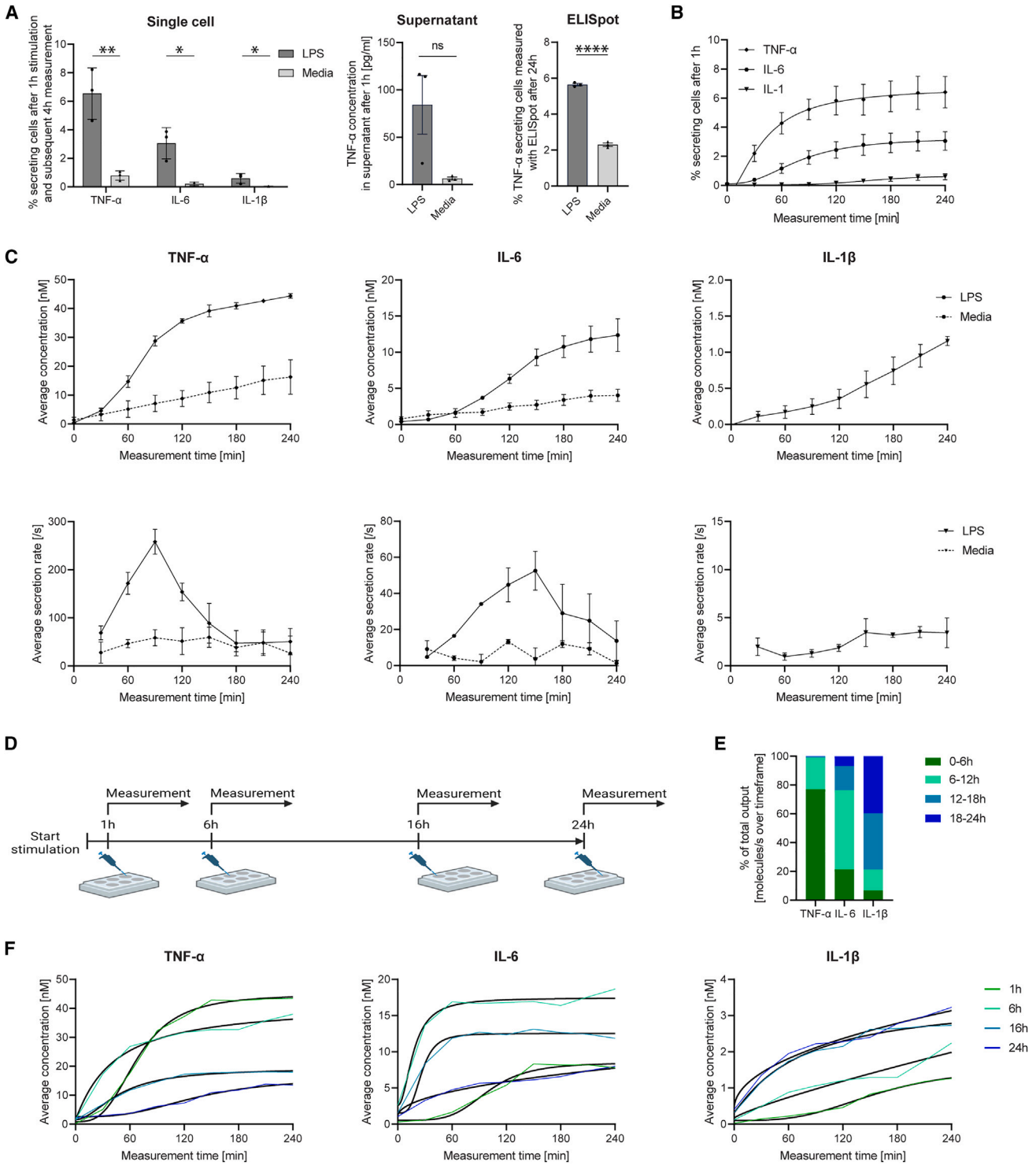

Figure 2. LPS stimulation of PBMCs revealed distinct secretion dynamics for TNF-α, IL-6, and IL-1β

(A) Percentage of TNF-α-, IL-6-, and IL-1β-secreting cells after 1-h stimulation with 1 μg/mL LPS (dark-gray bars) and no stimulant (light-gray bars) as measured by the microfluidic system at the end of the 4-h measurement (n = 3) (left). Respective controls for the supernatant measurements after 1-h stimulation (n = 3) with the same cells at 10^6 cells/mL (middle), and using ELISpot (24 h incubation, n = 1, N = 3) (right).

(B) Frequency of identified CSCs plotted against measurement time for all measured cytokines (only stimulated samples shown, n = 3).

(legend continued on next page)

the stimulated cells showed a sigmoidal increase in secreted TNF-α in the first 2 h and later displayed a linear increase similar to the background secretion in unstimulated cells (0.06 ± 0.03 vs. 0.16 ± 0.05 nM/min, p = 0.2). The maximal secretion rate for TNF-α was observed after 90 min, whereas a sharp increase and decrease in the average secretion rate was found around this time point. For IL-6, the average concentration showed an initial lag phase until 60 min, when the stimulated cells started to produce more IL-6 than the unstimulated control. The maximal IL-6 secretion rate was reached after 150 min. Conversely, IL-1β displayed a steady increase over time with no apparent plateau reached for concentration, with constant secretion rates from 150 to 240 min. Only a few IL-1β-secreting cells were found in the unstimulated cells (n < 10). Comparing the three cytokines, the maximal secretion rate was reached at different time points for TNF-α and IL-6 at 90 and 150 min, respectively, with secretion returning to basal levels (determined through unstimulated cells, dashed line in Figure 2C) after 4 h. IL-1β seemed to reach constant secretion after 150 min and did not revert to background levels within the measurement window. Of interest were also the vastly different amounts of secreted cytokines. At maximal secretion, TNF-α secretion was over 70-fold higher than IL-1β secretion.

Different stimulation times alter the frequency of CSCs and their secretion rates in a cytokine-specific manner

Given that in the previous application of DropMap the stimulation time was fixed to 3 h,[30] we next wanted to investigate the influence of stimulation time. Therefore, we stimulated PBMCs for various amounts of time with LPS in bulk, namely 1, 6, 16, and 24 h, and examined how cytokine secretion changed (Figures 2D–2F and S4A for unstimulated PBMCs). Indeed, the secreted fraction of the relative output varied for the different cytokines (Figure 2E), with TNF-α showing the highest output early (77%, 1 h), IL-6 intermediate (55%, 6 h), and IL-1β late (39%/40% after 16 h/24 h). Taking a closer look at the percentage of CSCs and secretion rates, we could observe a clear attenuation of secretion for TNF-α and IL-6 with prolonged stimulation times. The highest frequency of CSCs was reached after 1 h (8.2% for TNF-α and 3.9% for IL-6, Figure S4B), with the highest secretion rates observed after 6 h (276 and 156 molecules per second, respectively, Figure S4B). In contrast, IL-1β showed an increased number of activated cells and increased secretion with longer stimulation times, whereby the percentage and secretion rate reached a plateau after 16-h and 24-h stimulations (1.3% for both time points).

Most strikingly, different secretion dynamics were observed depending on the cytokine and stimulation time (Figure 2F, bottom). For better comparison, secretion dynamics were fitted with non-linear sigmoidal regression fits. TNF-α secretion showed different behavior depending on the stimulation time: 1 h led to an initial lag phase but reached the highest plateau during the measurement time (44.8 nM), whereas 6 h and 16 h showed a similar increase over time with lower plateau concentrations reached. Indeed, plateau concentrations negatively correlated with the duration of stimulation (44.8 nM, 41.7 nM, 19.3 nM, and 16.1 nM, respectively). The 24-h stimulation led to a slower increase, with a pronounced lag phase until 60 min and the lowest plateau concentration (16.1 nM). IL-6 showed the same dynamic after 6-h and 16-h incubations, with the highest plateau reached after 6 h of stimulation (17.5 nM). For this cytokine, time-resolved analysis allowed the discrimination of secretion behavior missed by traditional methods. Exemplarily for the 1-h and 24-h stimulations, almost identical endpoint concentrations were reached (7.8 nM and 8 nM, respectively, no fit of plateau possible for the 24-h measurement), but secretion after 1-h stimulation only started 60 min into the measurement. This difference was also observed in secretion-rate analysis (see Figure S4C). IL-1β, on the other hand, showed the same dynamics for all stimulation times, with increasing endpoint concentrations from 1 h to 24 h (1.3 nM, 2.2 nM, 2.7 nM, and 3.2 nM, respectively, no plateau reached during measurement time).

Differently pronounced lag phases of cytokine secretion were observed after only 1 h of stimulation, identified by fitting the IC_{50} values (69, 100, and 158 min for TNF-α, IL-6, and IL-1β, respectively). Attenuation of secretion for TNF-α and IL-6, but not for IL-1β, was also clearly apparent with longer incubation times, represented by decreasing plateau concentrations. Depending on the stimulation time, different dynamics were observed for TNF-α, IL-6, and IL-1β. Additionally, in-depth secretion measurements were possible with stimulation times as short as only 1 h.

Single-cell analysis resolved different distributions in the secretion level and identified binary and tertiary cellular responses

Dynamic single-cell resolution allowed the identification of different secretion behavior through the change of in-droplet concentration over the measurement time. Six randomly selected TNF-α-secreting cells are shown in Figure 3A after a 1-h stimulation with LPS. When comparing the cells depicted in green and orange, a similar secretion behavior was observed for up to 90 min. Thereafter, the cell depicted in green greatly increased its cytokine secretion, whereas the cell depicted in orange stopped secreting, resulting in different average secretion

(C) Average secreted concentration (top) and average secretion rates over measurement time (bottom) for all CSCs releasing TNF-α, IL-6, or IL-1β. Panels show the average of all three replicates from (A) with LPS (continuous line) and no added stimulant (dashed line) for TNF-α (n_{CSCs_pos} = 4,347, n_{CSCs_neg} = 295), IL-6 (n_{CSCs_pos} = 2,014, n_{CSCs_neg} = 78), and IL-1β (n_{CSCs_pos} = 383, n_{CSCs_neg} = 6). For n < 10, data are not displayed.
(D) Influence of different bulk stimulation times on cytokine secretion. PBMCs were incubated for 1, 6, 16, and 24 h, with subsequent measurements over 4 h.
(E) The relative output of every cytokine was normalized to the total output for all measurements per cytokine. For more information, refer to STAR Methods.
(F) Average secreted concentrations over the measurement time for different stimulation times (colored lines, n = 1) with the sigmoidal fit (black lines, GraphPad Prism, all fits R^2 > 0.935). Number of cells for 1, 6, 16, and 24 h, respectively: TNF-α: n_{CSCs_pos} = 1,827, 270, 47, 13; IL-6: n_{CSCs_pos} = 860, 187, 148, 124; IL-1β: n_{CSCs_pos} = 187, 86, 280, 239.
All experiments were performed with the same cell batch and stimulation. If not stated otherwise, data are depicted as mean ± SEM. (D) was created with BioRender.com. P values: * 0.05 – 0.01, ** 0.01 – 0.001, *** 0.001 – 0.0001, **** < 0.0001

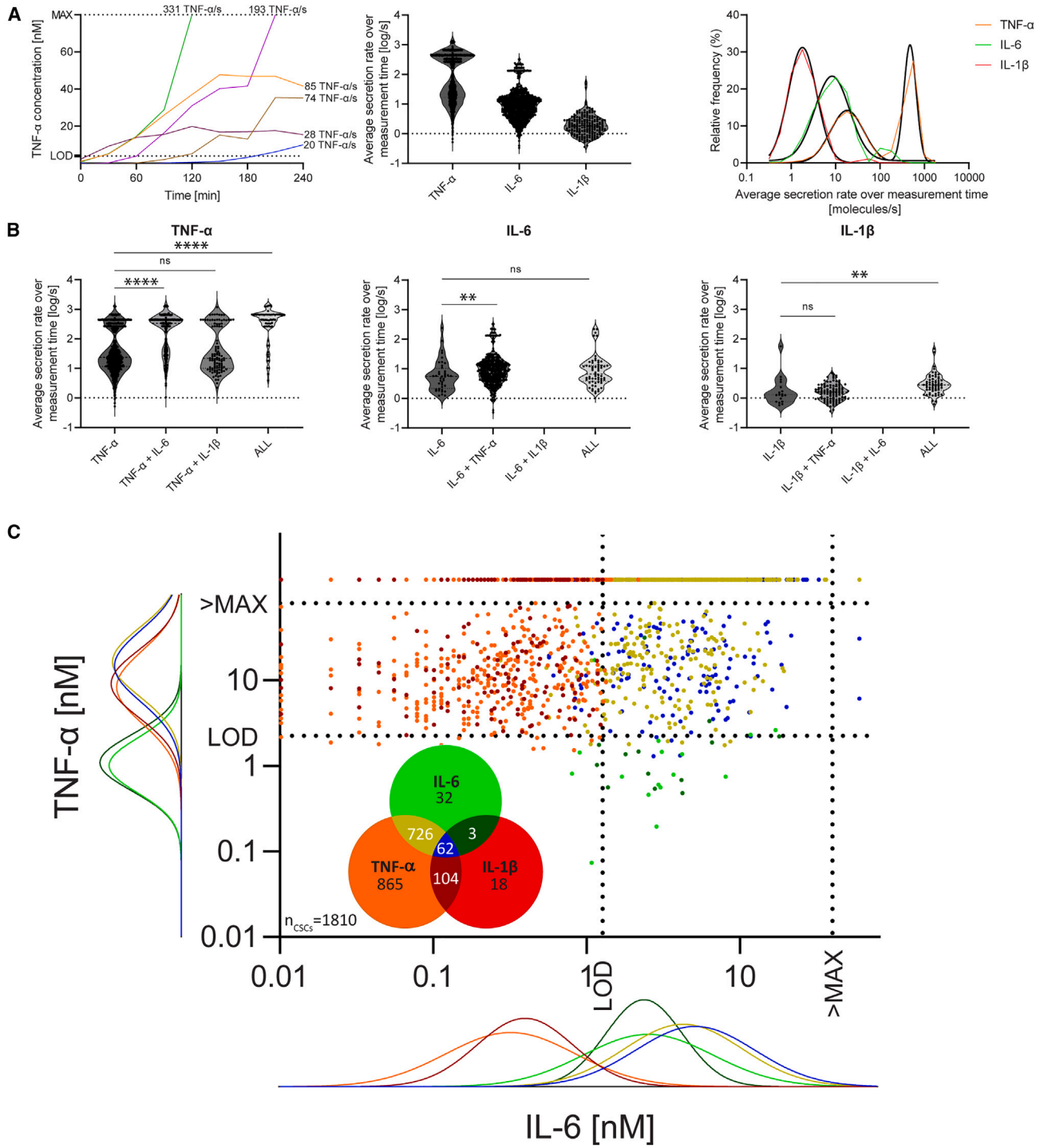

Figure 3. Secretion patterns, cellular subpopulations, and cytokine correlations in response to 1-h LPS stimulation

(A) In-droplet TNF-α concentration traces of selected representative CSCs over the measurement time. The maximum measurable concentration was 80 nM. The averaged secretion-rate (log) distributions over the 4-h measurement of one of the replicates shown in Figures 2A–2C (each dot represents a CSC, n_{CSCs} = 1,827 for TNF-α, n_{CSCs} = 860 for IL-6, and n_{CSCs} = 187 for IL-1β). Frequency distribution of the average secretion rates (log), binned in 0.25 bins (≈1.8 molecules per second), and fitted with the sum of two Gaussians (GraphPad Prism).

(B) Average secretion-rate (log) distributions for TNF-α-, IL-6-, and IL-1β secreting cells, divided based on co-secretion of cytokines. Statistical differences in secretion-rate distributions were assessed using two-sided, unpaired, nonparametric Kolmogorov-Smirnov tests with 95% confidence and $p < 0.05$. Data with fewer than ten detected co-secreting cells are not depicted.

(legend continued on next page)

rates over the measurement time (331 and 85 TNF-α molecules per second, respectively).

Next, we extracted the average secretion rates over the measurement time for every cytokine and single secreting cell (Figure 3A, second and third panels). Here, different distributions were observed for the different cytokines, with TNF-α clearly showing two distinct subpopulations with fitted population means at 18.2 and 474.2 molecules per second, respectively. IL-6 showed one distinct population with a mean of 8.3 molecules per second and a smaller subpopulation with a too-low sample size to be fitted correctly. IL-1β displayed a single secretion-rate distribution over the population with a mean of 1.8 molecules per second. Thus, the TNF-α-secreting cell population can be divided into low- and high-TNF-α secretors, with the caveat that the high-secreting population could be more spread out because almost all cells in this population (99%) reached the maximal measurable concentration of the assay during measurement.

Multiplex cytokine analysis allowed correlation of secretion patterns with co-secretion

By implementing multiplex cytokine secretion measurement in our method, we wanted to investigate whether the co-secretion of another cytokine influences the measured secretion rates. Again, we focused on the average secretion rates available for all cells and grouped them into whether or not the cells co-secrete other measured cytokines (Figure 3B). Differences in distribution were assessed with two-sided Kolmogorov-Smirnov t tests (unpaired, $p < 0.05$). For TNF-α-secreting cells, different secretion-rate distributions were identified for cells co-secreting IL-6 or all three cytokines simultaneously ($p < 0.0001$ for both) compared with TNF-α alone. This indicates that the co-secretion of IL-6 led to higher TNF-α secretion rates, whereas the co-secretion of IL-1β alone did not change secretion-rate distribution ($p = 0.5$). The reverse also seemed to be true for IL-6 to a certain extent. TNF-α co-secretion significantly altered the distribution ($p = 0.006$). However, the simultaneous secretion of all measured cytokines did not lead to a change ($p = 0.17$). IL-1β, on the other hand, showed a different behavior; only secretion of all three cytokines led to significantly increased IL-1β secretion ($p = 0.002$). Single co-secretion of TNF-α did not increase IL-1β secretion ($p = 0.5$).

The secretion data were further depicted in a phenotypic scatterplot (Figure 3C) comparing TNF-α and IL-6 endpoint concentrations of single- and co-secreting cells. Equal TNF-α and IL-6 endpoint concentration distributions were observed for single and co-secreting cells. This representation could be used to identify certain cell populations in the future, depending on their phenotype rather than cell-surface markers. After stimulating PBMCs for 1 h with LPS, most of the secreting cells secreted TNF-α only (49%) or TNF-α plus IL-6 (41%). Almost all of the IL-6- and IL-1β-secreting cells also co-secreted TNF-α (96% and 89%, respectively), as the populations of single secretors for those cytokines were very small. Only 62 cells (3%) secreted all three cytokines (Figure 3C, embedded Venn diagram).

Different stimulants induce specific dynamic cytokine responses

Next, we aimed to measure multiple cytokines in response to different stimulants reflecting the most commonly used positive controls in traditional CRAs (Figure 4A).[20] We simultaneously measured the cytokines IL-2, MIP-1α, IL-8, TNF-α, IL-6, and IFN-γ after a 1-h stimulation with each stimulant. These experiments allowed us to identify early stimulus-specific responses on the single-cell level.

First, we looked at the secretion of IL-8. This cytokine has been described as being involved in innate immune pathways.[31] Already in unstimulated cells, a considerable amount of IL-8 is secreted by a subpopulation. Stimulations using LPS, zymosan, and phorbol myristate acetate (PMA)/ionomycin increased the frequency of IL-8-secreting cells roughly 3-fold (Figure 4A), whereas only LPS and zymosan increased the average secretion rate and the output, compared with unstimulated cells. The average endpoint concentrations were similar for LPS- and zymosan-stimulated cells (Figure 4B, 40.0 nM and 39.0 nM, respectively), with a prolonged lag phase for the latter, resulting in a lower secretion rate with zymosan as a stimulant. This increase in secretion rate was mostly due to a high-secreting cell population (>100 molecules per second) that was only observed after stimulations with LPS and zymosan, which exceeded the dynamic range quickly. Phytohemagglutinin (PHA) was the only stimulant that seemed to decrease cellular IL-8 secretion. In summary, LPS and zymosan led to the induction of high-secreting cell populations and PMA/ionomycin only to an increase in the number of IL-8-secreting cells with lower secretion rates, while PHA even had a lowering effect on both.

TNF-α secretion seems to follow mechanisms similar to those of IL-8 secretion. PMA/ionomycin, LPS, zymosan, and, to a much smaller extent, PHA increased the frequency of TNF-α-secreting cells. Interestingly, only LPS and zymosan increased the average secretion rates, whereas PMA/ionomycin did not change secretion rates and PHA showed a decrease in the secretion rate of this cytokine. Consequently, only PMA/ionomycin, LPS, and zymosan increased TNF-α output considerably (Figure 4A). Here, LPS led to the highest secreted concentration, followed by zymosan which again showed an initial lag phase. However, TNF-α never reaches the same average concentrations when stimulated with zymosan compared with LPS over the measurement period (48.6 nM vs. 33.2 nM), indicating a longer lag phase for induction of secretion for TNF-α than IL-8. While the amount of secreted TNF-α seemed similar for the other stimulants, differences can be seen in how this plateau was reached. PMA/ionomycin and anti-CD3/anti-CD28 had more secretion early on and PHA stimulation even lowered the secreted concentration compared with unstimulated cells. These observations were also made at the single-cell level. In

(C) Phenotypic scatterplot showing in-droplet concentrations for TNF-α and IL-6 after 4 h of measurement. Each dot represents a secreting cell, and values exceeding the maximal measurable concentration are plotted as above maximum. The embedded Venn diagram shows the number of CSCs in every category, with the corresponding color code matching the scatterplot. Average concentration distributions (log) were plotted along the axes and grouped into the same categories as shown in the Venn diagram and scatterplot.
P values: * 0.05 – 0.01, ** 0.01 – 0.001, *** 0.001 – 0.0001, **** < 0.0001

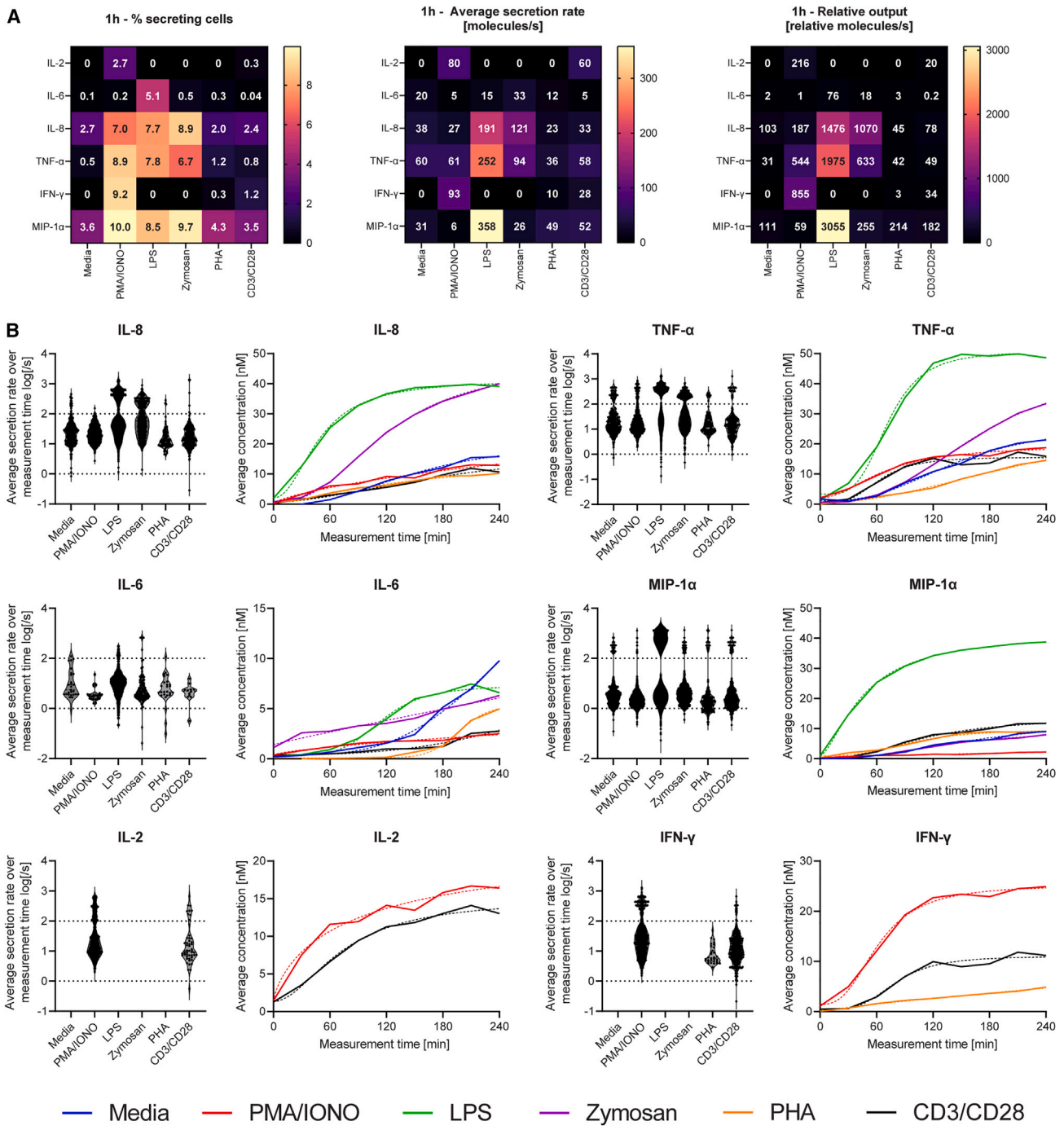

Figure 4. Influence of different stimulants on the level of cytokine secretion and their dynamics

(A) Heatmaps showing the percentage of secreting cells, averaged secretion rates (over measurement time for all secreting cells), and relative output measured after 1-h stimulation for all cytokines and stimulants.

(B) Average secretion-rate (log) distributions (each dot represents a CSC) and average cytokine concentrations over time for six selected cytokines and stimulants—IL-2, IL-6, IL-8, TNF-α, IFN-γ, and MIP-1α—in response to 1-h stimulations with 1 μg/mL LPS (green), 50 ng/mL PMA + 1 μg/mL ionomycin (red), 100 μg/mL zymosan (violet), 10 μg/mL PHA-L (orange), 5 μg/mL anti-CD3 (OKT3)/anti-CD28 (CD28.2, black), or medium alone (blue). Colored dotted lines show a sigmoidal fit (GraphPad Prism). Vertical dotted lines show secretion rates of 1 and 100 molecules per second, respectively. Data with fewer than ten detected secreting cells are not shown.

contrast to IL-8, high- and low-secreting populations were already present in unstimulated cells but increased considerably in LPS and zymosan stimulations (Figure 4B).

The frequency of IL-6-secreting cells only increased considerably after LPS stimulation and slightly after zymosan stimulation. Following the average concentration over time, a clear and early response to zymosan stimulation was visible, followed by LPS that showed a clearly delayed but stronger secretion, leading to similar average concentrations at the end of the measurement (6.6 nM vs. 6.3 nM), but with a higher average secretion rate for zymosan (Figure 4A). Interestingly, the unstimulated cells secrete high amounts of IL-6 at later time points, but the number of activated cells is much lower compared with zymosan or LPS stimulations (0.1% vs. 0.5% and 5.1%, respectively, Figure 4A). A clear shift in secretion-rate distribution was also observed for LPS compared with the other stimulants. Interestingly, compared with unstimulated cells, PMA/ionomycin and anti-CD3/anti-CD28 stimulations lowered the average concentrations at the population level (Figure 4B).

MIP-1α was already secreted by 3.6% of PBMCs in the unstimulated condition, which was increased by stimulations with PMA/ionomycin, zymosan, LPS, and PHA, respectively. Average secretion rates were only increased by LPS, PHA, and anti-CD3/anti-CD28 (Figure 4A). Regarding average concentrations over time, only LPS considerably increased the measured concentration compared with unstimulated cells. In contrast to measured IL-8 and TNF-α, zymosan did not induce higher MIP-1α secretion rates, and PMA/ionomycin even decreased secretion rates of MIP-1α. Interestingly, MIP-1α secretion seemed binary throughout all stimulations, showing a population of low-secreting cells (approximately ten molecules per second) and an additional high-secreting population (>1,000 molecules per second), especially prominent with LPS stimulation (16.2% compared with 0%–1.5% for the other stimulations, Figure 4B).

One-hour incubations with either PMA/ionomycin or anti-CD3/anti-CD28 showed a clear induction of specific cytokines, such as IL-2 and IFN-γ that are usually linked to adaptive immune responses.[32,33] For IL-2 the secretion-rate distributions are similar, but PMA/ionomycin activated 9-fold more cells and led to a slightly higher measured average concentration after 4 h of measurement (13.0 nM vs. 16.4 nM, respectively). For IFN-γ, there is a clear induction of a second higher-secreting cell population when stimulated with PMA/ionomycin, leading to a shift to higher average concentrations over time. Additionally, PHA also showed a clear induction of IFN-γ secretion, with fewer cells activated and a lower secretion rate than PMA/ionomycin and anti-CD3/anti-CD28 stimulations (Figure 4B). In terms of induction of IFN-γ secretion the stimulants can thus be ranked, with PMA/ionomycin being the most potent and PHA being the least potent. Generally, PMA/ionomycin activated the most cells in total (24%) for simultaneous measurements of IL-2, IL-8, and MIP-1α.

Activation dynamics showed distinct stimulant dependency early but not after prolonged stimulation

As described in Figure 2, the cellular cytokine response was strongly dependent on stimulation time. We, therefore, performed experiments with the most biologically relevant stimulus, anti-CD3/anti-CD28, in which PBMCs were incubated for 1 h and 24 h, and compared the results with cytokine concentrations measured in the supernatant for stimulated and unstimulated cells (Figure 5A). As expected, a 1-h stimulation was too short to increase cytokine concentrations in the supernatant, whereas the 24-h incubation increased the cytokine levels of IL-2, TNF-α, IFN-γ, and MIP-1α compared with unstimulated cells. Compared with the microfluidic measurement, we measured highly increased secretion of MIP-1α, TNF-α, IFN-γ, and IL-2 but decreased secretion for IL-8 with prolonged incubation, with secretion being detected already after 1 h. To assess the influence of prolonged bulk incubations on the dynamics of cytokine secretion, we exemplarily looked at TNF-α secretion for all the used stimulants (Figure 5B). Comparing 1-h with 24-h incubations, it was obvious that secretion reverted to background level for the LPS and zymosan conditions but remained above background (unstimulated) for PMA/ionomycin, anti-CD3/anti-CD28, and PHA stimulations, indicating a longer-lasting induction of TNF-α secretion probably from T cells.

Early stimulant-specific dynamics were lost with prolonged incubation times

Figure 5C shows the normalized frequencies, cellular secretion rates, and total output to compare long with short stimulations (24 h normalized to 1 h). As expected, the observed parameters changed for every cytokine and stimulation individually. IL-2 secretion was generally higher, with PMA/ionomycin leading to the strongest increase in total output. IL-6, on the other hand, decreased for LPS but increased for zymosan. Frequencies and secretion rates generally decreased for IL-8, except for PHA, which led to higher average secretion rates and increased total output. TNF-α secretion was generally also lower. Only PHA and anti-CD3/anti-CD28 stimulations increased the frequencies, secretion rates, and total output.

Similarly, IFN-γ secretion increased for these two stimulants, whereas PMA/ionomycin led to a decrease. Comparing these results with IL-2, IFN-γ seems to be expressed and upregulated earlier. MIP-1α secretion only decreased for unstimulated cells and LPS stimulations. A closer look at the concentration changes over measurement time for every cytokine and stimulant (Figure S5) revealed that the different dynamics were lost with 24-h stimulations, all showing a similar increase in concentration followed by a plateau. Depending on the stimulant, the plateaus came to lie at different heights. This could indicate a late response whereby additional stimulation due to cytokine secretion in bulk might appear, leading to a loss of individual secretion dynamics.

DISCUSSION

Current systems to measure cytokine release are typically highly multiplexed but endpoint measurements, and determine cytokine concentrations after prolonged incubation in bulk or on the single-cell level. Here, we wanted to establish a system capable of measuring cytokine secretion over different time points, enabling a dynamic resolution of secretion behavior of only a few selected cytokines at a time. For this we optimized our bioassays to measure three cytokines in parallel, including

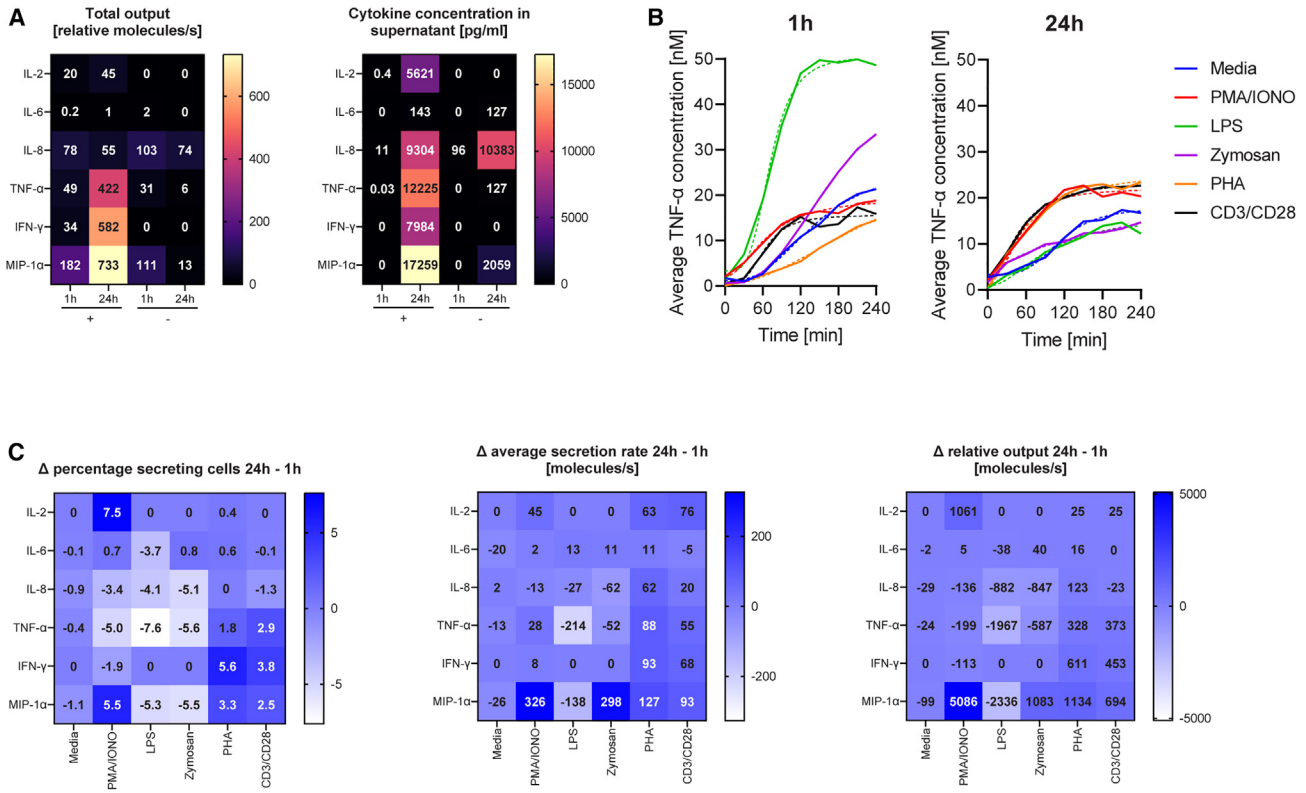

Figure 5. Comparison between 1-h and 24-h stimulations for measured cytokines.

(A) Heatmaps for relative output of the microfluidic measurement and measured concentrations in the supernatant (N = 2) of anti-CD3/anti-CD28 stimulated (+) and unstimulated cells (medium control, –) for 1-h and 24-h stimulations.

(B) Average TNF-α concentration over measurement time concerning all used stimulants for 1-h and 24-h stimulations. Dotted colored lines show a sigmoidal 4PL fit (GraphPad Prism).

(C) Heatmaps showing the normalized percentage of secreting cells, average secretion rates, and relative output after 24-h stimulations (normalized to 1-h stimulation, Figure 4A) for all cytokines and stimulants.

cytokines with significantly different secretion rates and levels. Consequently, the developed protocol allowed the determination of the frequency of CSCs, their secreted concentration, and their secretion rates, all in parallel and correlated with up to three secreted cytokines, identifying specific subpopulations within the measured cells.

We captured detailed behavior of cytokine secretion for measured TNF-α, IL-6, and IL-1β and identified an optimal measurement window for each (Figure 2), demonstrating the need to tailor assay sensitivity and dynamic range to the secretion rate of every cytokine. Compared to traditional assays, our approach was able to extract dynamic, detailed, and quantitative information and detect cytokine release shortly after stimulation. Similar trends measured in supernatant have been shown previously, but not as early as a 1-h stimulation.[19,34] To highlight advances and compare our method with existing technologies, we put together a table with the most established cytokine measurement techniques (Table S4). In short, dynamic single-cell resolution allowed us to identify when most cells are active and when the activated cells secrete the highest quantity of cytokines, showing that the number of activated cells and amount of secretion did not correlate for TNF-α and IL-6 but did for IL-1β for the chosen stimulation times. Therefore, different stimulation times should be considered depending on the cytokine and parameter of interest. Moreover, with many methods unable to resolve measurable concentrations early, selecting the appropriate measurement method is just as important as choosing the correct measurement window.

In addition to increased sensitivity and shorter measurement times, single-cell resolution allowed the extraction of additional information about every individual secreting cell. These single-cell data were captured over the time course of the measurement. Different average secretion-rate distributions were identified for TNF-α, IL-6, and IL-1β, with TNF-α showing a clear division into a high- and low-secreting population following a 1-h stimulation with LPS (Figure 3). The percentage of TNF-α-secreting cells (Figure 2A) could indicate that these are activated monocytes,[35] with the high- and low-TNF-α-secreting cells being different monocyte subpopulations. However, different TNF-α secretion levels have only been described so far for PMA and non-PMA primed monocytes followed by LPS stimulation,[36] a stimulation protocol different from the one employed here.

The introduction of multiplexed secretion analysis allowed the simultaneous detection of up to three cytokines per single cell

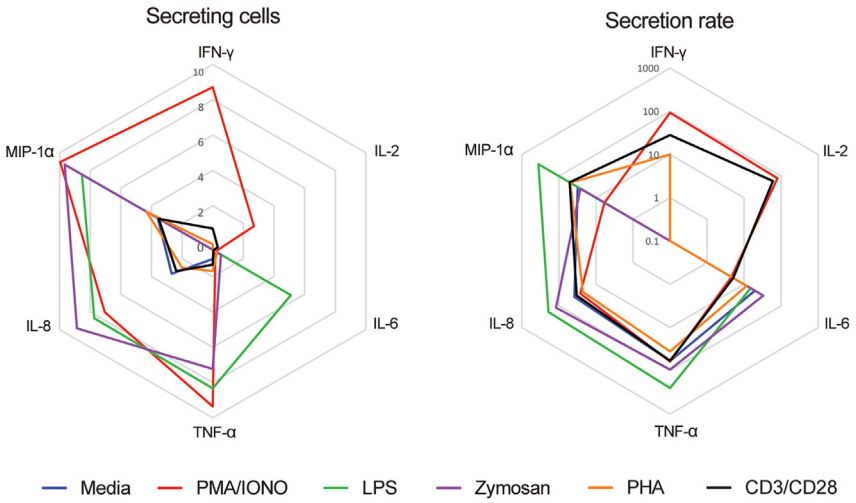

Figure 6. Radar diagrams for the early responses to different stimulants

Percentage of secreting cells and averaged secretion rates in molecules per second for the measured cytokines in response to 1-h stimulations with 1 μg/mL LPS (green), 50 ng/mL PMA + 1 μg/mL ionomycin (red), 100 μg/mL zymosan (violet), 10 μg/mL PHA-L (orange), 5 μg/mL anti-CD3 (OKT3) + anti-CD28 (CD28.2, black) or medium alone without added stimulant (blue).

over time. Thus, a heterogeneous cell set, such as PBMCs, could be classified and grouped based on the secreted cytokines. TNF-α secretion increased significantly when IL-6 was co-secreted by the cell, but the co-secretion of IL-1β did not change the level of secretion or the distribution thereof. IL-6 co-secretion coincided with the high-secreting population of TNF-α-secreting cells. However, various immune cells secrete IL-6, and it is difficult to assign cellular populations to these secretion patterns.[37] IL-6 secretion followed a similar behavior; cells that co-secreted TNF-α had a significantly higher amount of IL-6 secretion than cells not secreting TNF-α, so a clear link between co-secretion and increased cytokine levels could be observed. LPS acts via Toll-like receptor 4 (TLR4) signaling, which has also been described for monocytes and T cells, whose exact function is still unclear because pro- and anti-inflammatory effects have both been observed.[38–40] Therefore, the observed populations probably consist of monocytes, T cells, or a mixture thereof, and further characterization would be necessary. Enrichment for one of these populations, followed by subsequent measurement with our approach, could give clearer results for the phenotypic activity of TLR4-activated T cells and monocytes. Enrichment of the target population of interest could be beneficial to improve the readout, especially for weaker or selective stimulants.

IL-1β, on the other hand, seems to be exclusively secreted by monocytes,[41] so secretion thereof could be an identification marker for these cells. Two subpopulations were identified, with cells secreting TNF-α, IL-6, and IL-1β at once, having a significantly increased secretion of IL-1β. Different secretion levels of these cytokines have been identified for monocyte subpopulations, with non-classical monocytes secreting the most IL-1β.[42] However, it cannot be confirmed that these cells co-secrete IL-6 and TNF-α because these experiments were performed in bulk. Generally, the method allows grouping of the cells based on their activity level and phenotype, potentially enabling the characterization of new cellular subsets (Figure 3). The method's usefulness could be additionally expanded by incorporating corresponding cell-surface markers or by establishing specific single-cell signatures for previously enriched cellular subsets.

Expanding the stimulants to typically used positive controls in CRAs[20] already yielded specific responses after a 1-h stimulation. Interestingly, the percentage of CSCs and average secretion rates did not correlate for different stimulants and cytokines compared with unstimulated cells (Figure 4). Generally the response aligned with expectations, with TLR agonists such as LPS and zymosan leading to secretion of IL-6, IL-8, and TNF-α,[43–46] and T cell-specific stimulants, such as anti-CD3/anti-CD28 and PHA, leading to secretion of IL-2 and IFN-γ.[47–49] PMA/ionomycin is a well-known activation cocktail for immune cells to induce cytokine secretion,[50–52] so the broad and stronger cytokine response we observed is probably from a mixture of different activated cell types. However, our methodology uncovered different secretion dynamics in response to different stimulants. An example would be the IL-8 response to LPS and zymosan: the same endpoint concentration was reached after the measurement time, but zymosan led to a delayed secretion, which strongly increased later in the measurement. Observing the different dynamics can also help to identify the potency of stimulants.

To check for differences in early and late responses, the experiments were repeated with 24-h stimulations (Figures 5 and S5). The prolonged incubation led to similar dynamics for all the measured cytokines and stimulants, with different endpoint concentrations reached depending on the stimulant. These differences could indicate how strong and long a stimulus induces a specific cytokine response, with secondary stimulations through the secreted cytokines in bulk probably influencing secretion. TNF-α, highly secreted in all measured stimulations, can have pro- and anti-inflammatory effects and act on various immune cells,[53] which might alter the measured response with longer stimuli. Therefore, we hypothesize that especially short stimulations and the measured response can give insights into the activation and underlying mechanism. This could allow classifying the early response when testing other stimulants; for example, anti-CD3/anti-CD28 and PMA/ionomycin had similar responses when examining the average secretion rates of IL-2 and IFN-γ but not when considering percentage of secreting cells (Figure 6). This difference could be due to T cells stemming from differently activated cellular subpopulations in response to PMA/ionomycin and anti-CD3/anti-CD28. Alternatively, this could be another cellular subset not activated by anti-CD3/anti-CD28 stimulation, such as natural killer cells that do not possess a T cell receptor, or even macrophages, which have

been reported to secrete IFN-γ, but only if the stimulation included IL-12 and IL-18.[54] The loss of individual secretion dynamics could also be because the cells were still mounting a response after 1 h but reached equilibrium after a 24-h stimulation, aligning with reports showing increased gene expression up to 8 h after stimulations with PHA and anti-CD3 antibodies in PBMCs.[55] Therefore, prolonged stimulation times could give insights into an established secretion equilibrium in bulk. This equilibrium was especially prominent for TNF-α, where all stimulants also known to activate T cells led to prolonged and increased cytokine secretion compared with unstimulated and LPS/zymosan-stimulated cells (Figure 5B).

Limitations of the study

Limitations of the method include that our single-cell measurements do not allow for further manipulation of the cells after encapsulation. Therefore, the addition or removal of stimulants is presently not possible. Additionally, single-cell microfluidic assays inherently limit contact-based and paracrine cell-cell interactions during the measurement, an eventuality that prolonged bulk incubations ahead of encapsulation could partly mediate. Autocrine effects from secreted cytokines on single encapsulated cells cannot be excluded, owing to potential influences of unmeasured cytokines and analytes, and their extent and influence will likely depend on stimulation and cytokine. Therefore, because of platform-specific differences, only limited comparability of the droplet-based method is possible with existing methods such as ELISA and ELISpot. However, if of interest, the image-based technique described herein allows differentiating singlets from doublets and multiplets, adding dimensionality to the presented approach (Figure S2B). An isolated view on cytokine secretion might be useful for certain questions, specifically considering only local cellular secretion in tissues. Here, we expect the secreted cytokine to accumulate around the secreting cell, limiting contact and paracrine effects and potentially leading to enhanced autocrine effects. This setup will likely not recapitulate other *in vivo* situations, such as secretion in blood whereby cytokines are diluted and removed from the cell's vicinity immediately. Lastly, the assay's dynamic range in the droplet is limited, and high-secreting cells can exceed the upper capacity limit, potentially influencing the results (47% at maximum usually 5%–20% in this study). The secretion dynamics and trends described in this study were also apparent in analyzed low-secreting cell populations (i.e., excluding the cells reaching the calibration maximum, data not shown), excluding a potential bias due to assay saturation.

Conclusions

In summary, our methodology identified phenotypically different subpopulations in stimulated PBMCs (Figure 3) and resolved differences between early and late secretion responses to various stimuli, differences that were masked using conventional methods. Therefore, our protocol greatly improves the previously published DropMap technology and is a valuable addition to traditional CRAs,[20] especially with the recent rise of new therapies and formats that interact with and manipulate the immune system.[10,56] The quantitative insights into secretion dynamics on the single-cell level might also enable interested researchers to engage with new fundamental and applied research questions. For example, pre-sorted T cell subpopulations or innate immune cells could be analyzed in detail. This would allow researchers to disentangle levels of functionality between and within different cell types. From a more applied angle, we see interesting applications of these assays in questions where the dynamics and level of secretion might be fundamental. Irregular cytokine secretion behavior has been associated with various diseases and infections, such as HIV and cancer.[37,57,58] The assay could be used for the detection and understanding of aberrant and overshooting cytokine responses, such as CRS. Indeed, the dynamic resolution of the method might be useful to investigate the different stages of CRS and to unravel their origins and evolution over time. As imbalances are associated with disease states, the protocol might also be used in routine patient point-of-care testing in clinical settings. There, phenotypic and especially quantitative, dynamic, and functional characterization of these irregular secretion patterns could prove beneficial in understanding the pathology and underlying mechanisms, enabling the possibility of personalized treatment and earlier diagnosis.

STAR★METHODS

Detailed methods are provided in the online version of this paper and include the following:

- KEY RESOURCES TABLE
- RESOURCE AVAILABILITY
  - Lead contact
  - Materials availability
  - Data and code availability
- EXPERIMENTAL MODEL AND SUBJECT DETAILS
- METHOD DETAILS
  - PBMC isolation and freezing
  - PBMC thawing and stimulation
  - Cell suspensions for droplet generation
  - Nanoparticle and reagent solutions
  - Observation chamber assembly and PDMS chip production
  - Droplet production and immobilization
  - Imaging and data acquisition
  - Data analysis
  - Calibration curves for different cytokine panels
  - Human TNF-α ELISpot
  - Cytokine supernatant measurements
- QUANTIFICATION AND STATISTICAL ANALYSIS

SUPPLEMENTAL INFORMATION

Supplemental information can be found online at https://doi.org/10.1016/j.crmeth.2023.100502.

ACKNOWLEDGMENTS

The authors wish to thank Nathan Aymerich and Guilhem Chenon for their support in the original code used in this study. This project was supported by grant #2021-349 of the Strategic Focus Area "Personalized Health and Related

Technologies (PHRT)" of the ETH Domain (Swiss Federal Institutes of Technology), the Swiss National Foundation, "Olga Mayenfisch Stiftung," and the Novartis Foundation for medical-biological research.

AUTHOR CONTRIBUTIONS

Design of research: K.P. and K.E. Performed experiments: K.P., A.L., and N.O. Analyzed data: K.P. Wrote the manuscript: K.P. and K.E. All authors revised and commented on the manuscript.

DECLARATION OF INTERESTS

K.E. is a co-inventor on patents related to single-cell analysis and is a co-founder of Saber Bio SAS. K.E. has received consulting fees from the company.

INCLUSION AND DIVERSITY

We support inclusive, diverse, and equitable conduct of research.

Received: February 13, 2023
Revised: March 31, 2023
Accepted: May 23, 2023
Published: June 14, 2023

REFERENCES

1. Banyer, J.L., Hamilton, N.H., Ramshaw, I.A., and Ramsay, A.J. (2000). Cytokines in innate and adaptive immunity. Rev. Immunogenet. *2*, 359–373.
2. Imanishi, J. (2000). Expression of cytokines in bacterial and viral infections and their biochemical aspects. J. Biochem. *127*, 525–530. https://doi.org/10.1093/oxfordjournals.jbchem.a022636.
3. Peiris, J.S.M., Guan, Y., and Yuen, K.Y. (2004). Severe acute respiratory syndrome. Nat. Med. *10*, S88–S97. https://doi.org/10.1038/nm1143.
4. Gödel, P., Shimabukuro-Vornhagen, A., and von Bergwelt-Baildon, M. (2018). Understanding cytokine release syndrome. Intensive Care Med. *44*, 371–373. https://doi.org/10.1007/s00134-017-4943-5.
5. Channappanavar, R., and Perlman, S. (2017). Pathogenic human coronavirus infections: causes and consequences of cytokine storm and immunopathology. Semin. Immunopathol. *39*, 529–539. https://doi.org/10.1007/s00281-017-0629-x.
6. Huang, K.J., Su, I.J., Theron, M., Wu, Y.C., Lai, S.K., Liu, C.C., and Lei, H.Y. (2005). An interferon-gamma-related cytokine storm in SARS patients. J. Med. Virol. *75*, 185–194. https://doi.org/10.1002/jmv.20255.
7. Hu, B., Huang, S., and Yin, L. (2021). The cytokine storm and COVID-19. J. Med. Virol. *93*, 250–256. https://doi.org/10.1002/jmv.26232.
8. Reuter, M.A., Pombo, C., and Betts, M.R. (2012). Cytokine production and dysregulation in HIV pathogenesis: lessons for development of therapeutics and vaccines. Cytokine Growth Factor Rev. *23*, 181–191. https://doi.org/10.1016/j.cytogfr.2012.05.005.
9. Wu, Y., Yue, B., and Liu, J. (2016). Lipopolysaccharide-induced cytokine expression pattern in peripheral blood mononuclear cells in childhood obesity. Mol. Med. Rep. *14*, 5281–5287. https://doi.org/10.3892/mmr.2016.5866.
10. Ceschi, A., Noseda, R., Palin, K., and Verhamme, K. (2020). Immune checkpoint inhibitor-related cytokine release syndrome: analysis of WHO global pharmacovigilance database. Front. Pharmacol. *11*, 557. https://doi.org/10.3389/fphar.2020.00557.
11. Doessegger, L., and Banholzer, M.L. (2015). Clinical development methodology for infusion-related reactions with monoclonal antibodies. Clin. Transl. Immunology *4*, e39. https://doi.org/10.1038/cti.2015.14.
12. Brudno, J.N., and Kochenderfer, J.N. (2016). Toxicities of chimeric antigen receptor T cells: recognition and management. Blood *127*, 3321–3330. https://doi.org/10.1182/blood-2016-04-703751.
13. Maude, S.L., Barrett, D., Teachey, D.T., and Grupp, S.A. (2014). Managing cytokine release syndrome associated with novel T cell-engaging therapies. Cancer J. *20*, 119–122. https://doi.org/10.1097/ppo.0000000000000035.
14. Kulkarni, H.S., and Kasi, P.M. (2012). Rituximab and cytokine release syndrome. Case Rep. Oncol. *5*, 134–141. https://doi.org/10.1159/000337577.
15. Chowdhury, F., Johnson, P.W., Glennie, M.J., and Williams, A.P. (2014). Ex vivo assays of dendritic cell activation and cytokine profiles as predictors of in vivo effects in an anti-human CD40 monoclonal antibody ChiLob 7/4 phase I trial. Cancer Immunol. Res. *2*, 229–240. https://doi.org/10.1158/2326-6066.Cir-13-0070.
16. Vessillier, S., Fort, M., O'Donnell, L., Hinton, H., Nadwodny, K., Piccotti, J., Rigsby, P., Staflin, K., Stebbings, R., Mekala, D., et al. (2020). Development of the first reference antibody panel for qualification and validation of cytokine release assay platforms – report of an international collaborative study. Cytokine. X *2*, 100042. https://doi.org/10.1016/j.cytox.2020.100042.
17. Attarwala, H. (2010). TGN1412: from discovery to disaster. J. Young Pharm. *2*, 332–336. https://doi.org/10.4103/0975-1483.66810.
18. Hanke, T. (2006). Lessons from TGN1412. Lancet *368*, 1569–1570; author reply 1570. https://doi.org/10.1016/S0140-6736(06)69651-7.
19. Janský, L., Reymanová, P., and Kopecký, J. (2003). Dynamics of cytokine production in human peripheral blood mononuclear cells stimulated by LPS or infected by Borrelia. Physiol. Res. *52*, 593–598.
20. Finco, D., Grimaldi, C., Fort, M., Walker, M., Kiessling, A., Wolf, B., Salcedo, T., Faggioni, R., Schneider, A., Ibraghimov, A., et al. (2014). Cytokine release assays: current practices and future directions. Cytokine *66*, 143–155. https://doi.org/10.1016/j.cyto.2013.12.009.
21. Findlay, L., Eastwood, D., Stebbings, R., Sharp, G., Mistry, Y., Ball, C., Hood, J., Thorpe, R., and Poole, S. (2010). Improved in vitro methods to predict the in vivo toxicity in man of therapeutic monoclonal antibodies including TGN1412. J. Immunol. Methods *352*, 1–12. https://doi.org/10.1016/j.jim.2009.10.013.
22. Stebbings, R., Eastwood, D., Poole, S., and Thorpe, R. (2013). After TGN1412: recent developments in cytokine release assays. J. Immunotoxicol. *10*, 75–82. https://doi.org/10.3109/1547691x.2012.711783.
23. Römer, P.S., Berr, S., Avota, E., Na, S.Y., Battaglia, M., ten Berge, I., Einsele, H., and Hünig, T. (2011). Preculture of PBMCs at high cell density increases sensitivity of T-cell responses, revealing cytokine release by CD28 superagonist TGN1412. Blood *118*, 6772–6782. https://doi.org/10.1182/blood-2010-12-319780.
24. Smedman, C., Gårdlund, B., Nihlmark, K., Gille-Johnson, P., Andersson, J., and Paulie, S. (2009). ELISpot analysis of LPS-stimulated leukocytes: human granulocytes selectively secrete IL-8, MIP-1β and TNF-α. J. Immunol. Methods *346*, 1–8. https://doi.org/10.1016/j.jim.2009.04.001.
25. Ioannidou, K., Baumgaertner, P., Gannon, P.O., Speiser, M.F., Allard, M., Hebeisen, M., Rufer, N., and Speiser, D.E. (2017). Heterogeneity assessment of functional T cell avidity. Sci. Rep. *7*, 44320. https://doi.org/10.1038/srep44320.
26. Bucheli, O.T.M., Sigvaldadóttir, I., and Eyer, K. (2021). Measuring single-cell protein secretion in immunology: technologies, advances, and applications. Eur. J. Immunol. *51*, 1334–1347. https://doi.org/10.1002/eji.202048976.
27. Schoof, E.M., Furtwängler, B., Üresin, N., Rapin, N., Savickas, S., Gentil, C., Lechman, E., Keller, U.a.d., Dick, J.E., and Porse, B.T. (2021). Quantitative single-cell proteomics as a tool to characterize cellular hierarchies. Nat. Commun. *12*, 3341. https://doi.org/10.1038/s41467-021-23667-y.
28. Liu, Y.-C., Ansaryan, S., Li, X., Arvelo, E.R., and Altug, H. (2022). Real-time monitoring of single-cell secretion with a high-throughput nanoplasmonic microarray. Biosens. Bioelectron. *202*, 113955. https://doi.org/10.1016/j.bios.2021.113955.
29. Bounab, Y., Eyer, K., Dixneuf, S., Rybczynska, M., Chauvel, C., Mistretta, M., Tran, T., Aymerich, N., Chenon, G., Llitjos, J.F., et al. (2020). Dynamic single-cell phenotyping of immune cells using the microfluidic platform

DropMap. Nat. Protoc. *15*, 2920–2955. https://doi.org/10.1038/s41596-020-0354-0.

30. Llitjos, J.F., Bounab, Y., Rousseau, C., Dixneuf, S., Rimbault, B., Chiche, J.D., Textoris, J., Pène, F., and Védrine, C. (2021). Assessing the functional heterogeneity of monocytes in human septic shock: a proof-of-concept microfluidic assay of TNFα secretion. Front. Immunol. *12*, 686111. https://doi.org/10.3389/fimmu.2021.686111.
31. Bickel, M. (1993). The role of interleukin-8 in inflammation and mechanisms of regulation. J. Periodontol. *64*, 456–460.
32. Bendickova, K., and Fric, J. (2020). Roles of IL-2 in bridging adaptive and innate immunity, and as a tool for cellular immunotherapy. J. Leukoc. Biol. *108*, 427–437. https://doi.org/10.1002/jlb.5mir0420-055r.
33. Schoenborn, J.R., and Wilson, C.B. (2007). Regulation of interferon-gamma during innate and adaptive immune responses. Adv. Immunol. *96*, 41–101. https://doi.org/10.1016/s0065-2776(07)96002-2.
34. Schildberger, A., Rossmanith, E., Eichhorn, T., Strassl, K., and Weber, V. (2013). Monocytes, peripheral blood mononuclear cells, and THP-1 cells exhibit different cytokine expression patterns following stimulation with lipopolysaccharide. Mediators Inflamm. *2013*, 697972. https://doi.org/10.1155/2013/697972.
35. (2015). Peripheral blood mononuclear cells. In The Impact of Food Bioactives on Health: in vitro and ex vivo models, K. Verhoeckx, P. Cotter, I. López-Expósito, C. Kleiveland, T. Lea, A. Mackie, T. Requena, D. Swiatecka, and H. Wichers, eds. (Springer), pp. 161–167. https://doi.org/10.1007/978-3-319-16104-4.
36. Takashiba, S., Van Dyke, T.E., Amar, S., Murayama, Y., Soskolne, A.W., and Shapira, L. (1999). Differentiation of monocytes to macrophages primes cells for lipopolysaccharide stimulation via accumulation of cytoplasmic nuclear factor kappaB. Infect. Immun. *67*, 5573–5578. https://doi.org/10.1128/iai.67.11.5573-5578.1999.
37. Mauer, J., Denson, J.L., and Brüning, J.C. (2015). Versatile functions for IL-6 in metabolism and cancer. Trends Immunol. *36*, 92–101. https://doi.org/10.1016/j.it.2014.12.008.
38. Zanin-Zhorov, A., and Cohen, I.R. (2013). Signaling via TLR2 and TLR4 directly down-regulates T cell effector functions: the regulatory face of danger signals. Front. Immunol. *4*, 211. https://doi.org/10.3389/fimmu.2013.00211.
39. Reynolds, J.M., Martinez, G.J., Chung, Y., and Dong, C. (2012). Toll-like receptor 4 signaling in T cells promotes autoimmune inflammation. Proc. Natl. Acad. Sci. USA *109*, 13064–13069. https://doi.org/10.1073/pnas.1120585109.
40. Koch, L., Frommhold, D., Buschmann, K., Kuss, N., Poeschl, J., and Ruef, P. (2014). LPS- and LTA-induced expression of IL-6 and TNF-α in neonatal and adult blood: role of MAPKs and NF-κB. Mediators Inflamm. *2014*, 283126. https://doi.org/10.1155/2014/283126.
41. Dinarello, C.A. (2005). Blocking IL-1 in systemic inflammation. J. Exp. Med. 201, 1355-1359. https://doi.org/10.1084/jem.20050640.
42. Wong, K.L., Tai, J.J.-Y., Wong, W.-C., Han, H., Sem, X., Yeap, W.-H., Kourilsky, P., and Wong, S.-C. (2011). Gene expression profiling reveals the defining features of the classical, intermediate, and nonclassical human monocyte subsets. Blood *118*, e16–e31. https://doi.org/10.1182/blood-2010-12-326355.
43. Flynn, C.M., Garbers, Y., Lokau, J., Wesch, D., Schulte, D.M., Laudes, M., Lieb, W., Aparicio-Siegmund, S., and Garbers, C. (2019). Activation of toll-like receptor 2 (TLR2) induces interleukin-6 trans-signaling. Sci. Rep. *9*, 7306. https://doi.org/10.1038/s41598-019-43617-5.
44. Gvirtz, R., Ogen-Shtern, N., and Cohen, G. (2020). Kinetic cytokine secretion profile of LPS-induced inflammation in the human skin organ culture. Pharmaceutics *12*, 299. https://doi.org/10.3390/pharmaceutics12040299.
45. Dillon, S., Agrawal, S., Banerjee, K., Letterio, J., Denning, T.L., Oswald-Richter, K., Kasprowicz, D.J., Kellar, K., Pare, J., van Dyke, T., et al. (2006). Yeast zymosan, a stimulus for TLR2 and dectin-1, induces regulatory antigen-presenting cells and immunological tolerance. J. Clin. Invest. *116*, 916–928. https://doi.org/10.1172/jci27203.
46. Sato, M., Sano, H., Iwaki, D., Kudo, K., Konishi, M., Takahashi, H., Takahashi, T., Imaizumi, H., Asai, Y., and Kuroki, Y. (2003). Direct binding of toll-like receptor 2 to zymosan, and zymosan-induced NF-κB activation and TNF-α secretion are down-regulated by lung collectin surfactant protein A1. J. Immunol. *171*, 417–425. https://doi.org/10.4049/jimmunol.171.1.417.
47. Trickett, A., and Kwan, Y.L. (2003). T cell stimulation and expansion using anti-CD3/CD28 beads. J. Immunol. Methods *275*, 251–255. https://doi.org/10.1016/s0022-1759(03)00010-3.
48. Green, J.A., Cooperband, S.R., and Kibrick, S. (1969). Immune specific induction of interferon production in cultures of human blood lymphocytes. Science *164*, 1415–1417. https://doi.org/10.1126/science.164.3886.1415.
49. Liao, W., Lin, J.-X., and Leonard, W.J. (2011). IL-2 family cytokines: new insights into the complex roles of IL-2 as a broad regulator of T helper cell differentiation. Curr. Opin. Immunol. *23*, 598–604. https://doi.org/10.1016/j.coi.2011.08.003.
50. Grievink, H.W., and Moerland, M. (2018). Sample aging profoundly reduces monocyte responses in human whole blood cultures. J. Immunol. Res. *2018*, 8901485. https://doi.org/10.1155/2018/8901485.
51. Röth, D., Krammer, P.H., and Gülow, K. (2014). Dynamin related protein 1-dependent mitochondrial fission regulates oxidative signalling in T cells. FEBS Lett. *588*, 1749–1754. https://doi.org/10.1016/j.febslet.2014.03.029.
52. Ai, W., Li, H., Song, N., Li, L., and Chen, H. (2013). Optimal method to stimulate cytokine production and its use in immunotoxicity assessment. Int. J. Environ. Res. Public Health *10*, 3834–3842. https://doi.org/10.3390/ijerph10093834.
53. Mehta, A.K., Gracias, D.T., and Croft, M. (2018). TNF activity and T cells. Cytokine *101*, 14–18. https://doi.org/10.1016/j.cyto.2016.08.003.
54. Darwich, L., Coma, G., Peña, R., Bellido, R., Blanco, E.J.J., Este, J.A., Borras, F.E., Clotet, B., Ruiz, L., Rosell, A., et al. (2009). Secretion of interferon-gamma by human macrophages demonstrated at the single-cell level after costimulation with interleukin (IL)-12 plus IL-18. Immunology *126*, 386–393. https://doi.org/10.1111/j.1365-2567.2008.02905.x.
55. Fan, J., Nishanian, P., Breen, E.C., McDonald, M., and Fahey, J.L. (1998). Cytokine gene expression in normal human lymphocytes in response to stimulation. Clin. Diagn. Lab. Immunol. *5*, 335–340. https://doi.org/10.1128/cdli.5.3.335-340.1998.
56. Hosseinkhani, N., Derakhshani, A., Kooshkaki, O., Abdoli Shadbad, M., Hajiasgharzadeh, K., Baghbanzadeh, A., Safarpour, H., Mokhtarzadeh, A., Brunetti, O., Yue, S.C., et al. (2020). Immune checkpoints and CAR-T cells: the pioneers in future cancer therapies? Int. J. Mol. Sci. *21*, 8305. https://doi.org/10.3390/ijms21218305.
57. Merlini, E., Tincati, C., Biasin, M., Saulle, I., Cazzaniga, F.A., d'Arminio Monforte, A., Cappione, A.J., 3rd, Snyder-Cappione, J., Clerici, M., and Marchetti, G.C. (2016). Stimulation of PBMC and monocyte-derived macrophages via toll-like receptor activates innate immune pathways in HIV-infected patients on virally suppressive combination antiretroviral therapy. Front. Immunol. *7*, 614. https://doi.org/10.3389/fimmu.2016.00614.
58. Kaneko, N., Kurata, M., Yamamoto, T., Morikawa, S., and Masumoto, J. (2019). The role of interleukin-1 in general pathology. Inflamm. Regen. *39*, 12. https://doi.org/10.1186/s41232-019-0101-5.
59. Eyer, K., Doineau, R.C.L., Castrillon, C.E., Briseño-Roa, L., Menrath, V., Mottet, G., England, P., Godina, A., Brient-Litzler, E., Nizak, C., et al. (2017). Single-cell deep phenotyping of IgG-secreting cells for high-resolution immune monitoring. Nat. Biotechnol. *35*, 977–982. https://doi.org/10.1038/nbt.3964.

STAR★METHODS

KEY RESOURCES TABLE

REAGENT or RESOURCE	SOURCE	IDENTIFIER
Antibodies		
CD28 Monoclonal Antibody (CD28.2)	Thermo Fisher	Cat#16-0289-85; RRID: AB_468927
CD3 Monoclonal Antibody (OKT3)	Thermo Fisher	Cat#16-0037-85; RRID: AB_468855
See Table S2 for a list of used capture and detection antibodies.		
Biological samples		
Human blood	Blood Bank Zurich	N/A
Chemicals, peptides, and recombinant proteins		
Recombinant Human IL-2	Peprotech	Cat#200-02
Recombinant Human IL-8 (CXCL8)	Peprotech	Cat#200-08
Recombinant Human MIP-1α (CCL3)	Peprotech	Cat#300-08
Recombinant Human IFN-γ	Peprotech	Cat#300-02
Recombinant Human IL-6	Peprotech	Cat#200-06
Recombinant Human TNF-α	Peprotech	Cat#300-01A
Recombinant Human IL-1β	Peprotech	Cat#200-01B
Standard LPS, *E. coli* K12	Invivogen	Cat#tlrl-eklps
Phytohemagglutinin-L (PHA-L)	Thermo Fisher	Cat#00-4977-93
Zymosan A from *Saccharomyces cerevisiae*	Merck	Cat#Z4250
PMA	Merck	Cat#p1585
Ionomycin from *Streptomyces conglobatus*	Merck	Cat#I9657
Critical commercial assays		
ELISpot Flex: Human TNF-α (ALP)	MABTECH	Cat#3512-2A
Human TNF-alpha Quantikine ELISA Kit	R&D Systems	Cat#DTA00D
Software and algorithms		
Dropmap Analyzer	Bounab et al., 2020[29]	https://doi.org/10.1038/s41596-020-0354-0
Lambda counting script	Supplementary Information	
MATLAB R2020a	Mathworks	
NIS Elements	Nikon	
Other		
Bio-Adembeads Streptavidin plus 300nm	Ademtech	Cat#03233

RESOURCE AVAILABILITY

Lead contact

Further information and requests for resources and reagents should be directed to and will be fulfilled by the lead contact, Klaus Eyer (klaus.eyer@pharma.ethz.ch).

Materials availability

This study did not generate new unique reagents.

Data and code availability

- Datasets reported in this paper will be shared by the lead contact upon request.
- All original code is available in this paper's supplemental information.
- Any additional information required to reanalyze the data reported in this paper is available from the lead contact upon request.

EXPERIMENTAL MODEL AND SUBJECT DETAILS

All experiments were performed using PBMCs from anonymized, healthy donors and were carried out under ethics agreement EK 202-N-56, approved by the ETH Zurich ethics commission. Due to the anonymized samples, no information about sex, age, and gender was available. The herein-reported results were generated using cells from the same buffy coat.

METHOD DETAILS

PBMC isolation and freezing

Peripheral blood mononuclear cells (PBMCs) were extracted from a buffy coat obtained from the Zurich blood bank. Buffy coat was diluted 1:1 with PBS with added 2 mM EDTA and centrifuged at 1200g for 20 min over a Ficoll layer (GE Healthcare). PBMCs were collected, washed with phenol red-free RPMI 1640 (10% heat-inactivated FBS, 25 mM HEPES, 50 U/mL Pen/Strep, Gibco, termed cell buffer) and treated with BDPharmLyse (BD Biosciences) red blood cell lysis buffer for 5 min at RT. Afterward, the cells were washed and aliquoted in qualified heat-inactivated FBS (Gibco) containing 10% DMSO (Applichem) at 10^7 cells/vial, subsequently frozen and stored in liquid nitrogen until use. The same aliquots of buffy coat were used for all experiments.

PBMC thawing and stimulation

PBMCs were thawed at 37°C in pre-warmed cell buffer, washed two times and stained using 5 μM CellTrace violet (ThermoFisher) per 2×10^6 cells in PBS (-Ca^{2+}/−Mg^{2+}, Gibco) for 5 min at 37°C. After, the cells were treated with human FcR blocking reagent (Miltenyi Biotec) for 10 min at RT, washed, counted and diluted to a final concentration of 10^6 cells/mL. 2×10^6 cells were incubated for 1-, 6-, 16- or 24 h in cell buffer alone, or with added 1 μg/mL lipopolysaccharide (Invivogen), 50 ng/mL Phorbol-myristate-acetate and 1 μg/mL Ionomycin (both Sigma-Aldrich), 100 μg/mL zymosan (Sigma-Aldrich), 10 μg/mL phytohemagglutinin-L (ThermoFisher), or 5 μg/mL anti-CD3 (OKT3, ThermoFisher) and anti-CD28 (CD28.2, ThermoFisher). Incubations were performed in ultra-low attachment 6-well plates (Corning), and wells were thoroughly scraped after incubating to detach PBMCs.

Cell suspensions for droplet generation

After incubation, the cells were washed with pre-warmed cell buffer and the supernatant was collected for further analysis. Immediately before encapsulation, the cells were centrifuged and resuspended in pre-warmed cell buffer at a concentration of 8 to 16×10^6 cells/mL to give an average 0.2 to 0.4 cells/droplet. The cell suspension was immediately encapsulated to eliminate cross-contamination between droplets leading to an increased assay background signal.

Nanoparticle and reagent solutions

Magnetic nanoparticles (streptavidin plus, 300 nm diameter, Ademtech) were diluted 1 to 1 in PBS and the biotinylated capture antibodies were added at final concentrations of 167 nM (for the list, see Table S3). If not purchased directly biotinylated, capture antibodies were biotinylated in-house using the EZ-LINK-NHS-PEG4-Biotin kit (ThermoFisher), and aliquots were stored at −20°C. After capture antibody addition, the solution was incubated for 30 min at RT. To eliminate unbound streptavidin residues, the nanoparticles were resuspended and D-biotin (Fluorochem) was added at a final concentration of 10 μM with subsequent incubation for 5 min at RT. After incubation, the nanoparticles are collected using a magnet, the supernatant discarded and the nanoparticles resuspended in 0.5x the volume of PBS and 0.5x the volume of 10% pluronic F-127 (ThermoFisher) with subsequent incubation at RT for 30 min. The nanoparticles were again collected, the supernatant discarded and the particles resuspended in blocking buffer (RPMI 1640, 5% artificial CHO knockout serum, 1% Pen/Strep, 1% recombinant human serum albumin, 25 mM HEPES, 0.1% pluronic F-127, all ThermoFisher) for 30 min at RT. This protocol is repeated for every capture antibody specific to each cytokine separately. After this step, the particles can be stored for up to 1 week at 4°C.

For IL-6, TNF-α and IL-1β measurements, the nanoparticles were mixed at a 2:1:1 ratio, washed twice with cell buffer and resuspended in 0.5x of the initial volume. Fluorescently labeled detection antibodies were added immediately before use as the last step (for the list, see Table S3). Detection antibodies were either labeled from the manufacturer or labeled in-house using different Alexa Fluor NHS ester conjugates (ThermoFisher) at RT. The final concentrations of detection antibodies were 10.0 nM, 6.7 nM and 10.0 nM for IL-6, TNF-α and IL-1β, respectively (i.e., 2x of the final in-droplet concentrations). Immediately before encapsulation, the particles were resuspended thoroughly by mixing. For IFN-γ measurements, the anti-IFN-γ functionalized nanoparticles were added at the same ratio instead of IL-1β. The detection antibody was replaced with IFN-γ specific detection antibody at a final concentration of 10.7 nM. For IL-2, IL-8 and MIP-1α measurements, the protocol was performed with the corresponding capture antibodies, particles mixed at 1.66:1.33:1 ratio, washed twice with cell buffer and resuspended in 0.5x the initial volume. Final concentrations of 10 nM, 10 nM, and 12.3 nM corresponding detection antibodies were added for IL-2, IL-8 and MIP-1α, respectively.

Observation chamber assembly and PDMS chip production

The observation chamber and PDMS chips were prepared as described elsewhere.[29]

Droplet production and immobilization

Droplets were generated using a hydrodynamic flow-focusing PDMS chip as described previously.[29] The continuous phase consisted of 2% 008-Fluorosufactant (RAN Biotechnologies) in HFE-7500 fluorinated oil (3M). Aqueous phases consisted of nanoparticle solutions with reagents and either cell suspensions (cell experiments) or recombinant proteins (calibration). Flow rates were adjusted to 800 μL/h for the continuous phase and 200 μL/h for the aqueous phases to produce droplets of 65 pL in volume and 50 μm in diameter. All solutions are kept at RT to reduce unspecific activation of cytokine production. The generated droplets were routed to an observation chamber sandwiched by two block magnets (K&J Magnetics), and production stopped as soon as the chamber was full (typically 10 min). Because the chamber is slightly narrower (40 μm) than the droplet diameter, the droplets are immobilized throughout the measurement. The filled chamber was directly mounted onto an epifluorescence microscope (TI2 Eclipse, Nikon) for imaging.

Imaging and data acquisition

For imaging, a Nikon TI2 Eclipse epifluorescence microscope was used. Fluorescence was measured using appropriate band-pass filter sets (DAPI, FITC, TRITC, Cy5, all Semrock) and a SOLA LED light source (Lumencor). The sample was enclosed in a darkened cage incubator (Okolab) and imaged at 37°C and ambient oxygen concentrations. Images were acquired using a 10× objective (NA 0.45) and camera settings (Orca Fusion or R2, Hamamatsu) specific for each channel. An array of 12 × 12 images was acquired for every time point, where all channels were measured for one image, and then the stage moved to the next image. The samples were measured every 30 min for 4 h. Generated images were saved as.nd2 files and exported to a separate computer for data analysis.

Data analysis

Images were analyzed using a custom MATLAB script (Mathworks, version R2020A). Droplets were detected on the bright-field channel using a Hough transformation, and the beadline was identified by the brightest pixels in a vertical line on every fluorescence channel in the direction of the magnetic field as described elsewhere.[29,59]

Within each droplet, the average intensity on the beadline was divided by the average intensity of the background of the droplet, resulting in a robust readout called beadline relocation. Similarly, the script calculated a whole droplet positive pixel count above a threshold to identify if a droplet contains a cell. This threshold was set individually for every measurement corresponding to 1% of the brightest pixels of the signal intensity distribution on the DAPI channel. The script compares the location of every droplet at each time point and tracks them. Subsequently, all droplets with tracking of more than 10 pixels from the first to the last time point were excluded from the analysis. The total cell count was determined by an additional custom MATLAB script (see Data S1, supplemental information), in which droplets are randomly selected and displayed to the user, who manually determined the number of cells per droplet. The identified cell number is divided by the total droplets sorted, and the accurate λ value was determined. The analysis stops if the λ value is within 5% over the last 100 sorted droplets. Total cell count is calculated by multiplying the determined λ by the total number of analyzed droplets.

The following criteria were applied to classify whether a droplet contains a cytokine-secreting cell: Droplet contained a cell (DAPI positive pixel count >0), the beadline relocation increases over the measurement time (slope >0), the maximum beadline relocation is above the LOD of the measurement, calculated according to the following formula:

$$\mu_{Relocation\ t0} + 1.645 * 2 * \sigma_{BLK},$$

And the minimal change between maximum and minimum beadline relocation needed to be greater than:

$$1.645 * 2 * \sigma_{BLK}.$$

The standard deviation of the blank was acquired from the calibration dataset. The same criteria set is applied to the empty droplet population (DAPI positive pixel count = 0), and a false-positive percentage was calculated to verify the robustness of the analysis (usually around 0–10 events only, i.e., around 0.01 to 0.05%). Whenever less than 50 droplets were evaluated as positive by the criteria, they were checked by hand, and if less than 10 cells met the visual inspection criteria (no fluorescence aggregates, elongated beadline), they were not considered for further analysis.

The relocation is quantified using calibration curves for all droplets meeting the criteria in a given channel (corresponding to one cytokine). If a droplet meets the criteria in multiple channels, the cell is deemed a co-secreting cell, secreting multiple cytokines. For co-secreting events, a random subpopulation is evaluated manually for cell count per droplet and checked if a potential encapsulation of multiple cells affects the analyzed parameters (population of single encapsulated cells compared to multiple encapsulated cells).

For secretion rate calculations, the concentration change between two-time points was translated into molecules per second with the help of the droplet volume (65 pL), and the values were averaged either per time point for all CSCs (Figures 2C and S4C) or overall time points for one single cell (various violin plots shown in Figures). If the maximum quantifiable relocation was reached before the end of the experiment, the concentration was set to the maximum, and no further concentration was calculated. The secretion rate was only averaged up to this time point. Relative output was calculated by multiplying the determined percentage of secreting cells with the averaged secretion rates of the whole secreting cell population.

Calibration curves for different cytokine panels

Droplets were generated as described above. Recombinant proteins for IL-1β, IL-2, IL6, IL-8, TNF-α, IFN-γ and MIP-1α (all Peprotech) at various concentrations were used instead of cell suspensions. The proteins were used alone or together to exclude unspecific capture and detection antibodies binding. Images were taken in a 2 × 2 array, and two images were taken per concentration. Median relocation values were fitted (One-phase association, GraphPad Prism), and resulting equations were used to quantify the secretion data.

Human TNF-α ELISpot

ELISpot Plus: Human TNF-α (HRP) Kit (Mabtech) was used to determine the frequency of TNF-α according to the supplier's instructions. 3′125 to 50′000 cells per well were stimulated with 1 μg/mL LPS or RPMI without stimulant in triplicates. The plate was incubated for 24 h at 37°C. Images were taken on an ELR04 EliSpot reader (AID).

Cytokine supernatant measurements

TNF-α concentration in cell supernatants after 1-h LPS stimulations and unstimulated controls were measured using the Human TNF-alpha Quantikine ELISA Kit (R&D Systems) according to the supplier's instructions.

QUANTIFICATION AND STATISTICAL ANALYSIS

Replicates are depicted as mean ± SEM if not stated otherwise. Wherever specified, n relates to biological replicates or the number of cells per experiment. For ELISpot and Codeplex, technical triplicates were performed. Differences between stimulated and unstimulated conditions (Figure 2A) were assessed with unpaired two-sided t-tests with 95% confidence. Differences in distributions (Figures 3B and S2B) were assessed with two-sided, unpaired, nonparametric Kolmogorov-Smirnov tests with 95% confidence. Analysis performed in GraphPad Prism 9 (GraphPad Software). p-values: * 0.05–0.01, ** 0.01–0.001, *** 0.001–0.0001, **** <0.0001. n = number of biological replicates, N = number of technical replicates, n_{CSCs} = number of identified cytokine-secreting cells. Statistical details can be found in the figure legends and results sections.